Check for updates

Moments of Intra-Dome Velocity Distribution as Robust Predictors of Rupture Status in Cerebral Aneurysms

Alexandra Lauric, James E. Hippelheuser, Adel M. Malek

BACKGROUND: **Wall shear stress (WSS), the spatial gradient of flow velocity at luminal surface, has been employed for aneurysmal hemodynamic analysis, but it is sensitive to surface irregularities and noise. We devised a volumetric approach to evaluate discriminant power of intra-dome flow velocity distribution and modal analysis in rupture status determination compared with previously described WSS analysis.**

METHODS: **Catheter three-dimensional rotational angiographic datasets matched for volume were segmented in 20 sidewall aneurysms (10 ruptured), computational fluid dynamics simulations were performed, and velocity distributions were extracted from mesh-independent isometric sampling followed by moment analysis (mean, variance, skewness, and kurtosis). Univariate and multivariate analysis was used to evaluate discriminant performance of velocity moments. Sensitivity of velocity moments and WSS was evaluated to bleb presence and surface irregularity using digital bleb removal and surface noise addition.**

RESULTS: **Velocity moments of ruptured aneurysms showed higher skewness (2.45 ± 0.57 vs. 1.36 ± 0.82, $P = 0.003$) and kurtosis (11.83 ± 4.77 vs. 6.05 ± 4.65, $P = 0.01$) with lower mean (0.019 ± 0.01 vs. 0.038 ± 0.02, $P = 0.03$) compared with unruptured lesions; in multivariate modeling, skewness alone emerged as best predictor (area under the curve = 0.88). Bleb removal increased low WSS by 548%, and surface noise decreased it by 85.8% while having a smaller (<7%) effect on velocity skewness and kurtosis.**

CONCLUSIONS: **High aneurysm dome flow velocity skewness and kurtosis suggest an exponential distribution in ruptured lesions, with high peaks at low velocities, consistent with areas of slow flow. In contrast to WSS-based techniques, this approach is robust against surface variations, with promising improved rupture status discriminant performance that requires further validation in expanded future studies.**

INTRODUCTION

Understanding factors leading to rupture of cerebral aneurysms remains an active area of research and a clinical priority. Robust and accurate tools for rupture risk analysis and prediction allow clinicians to better balance the risks and benefits of treatment strategies.[1] Hemodynamics are considered a major contributor to aneurysm formation and rupture[1]; whereas many hemodynamic features have been proposed and evaluated,[2] research has focused on wall shear stress (WSS), the tangential force of flowing blood on the vessel surface.[3-9] WSS is not uniform on the dome, being low at blebs and high near the neck. High- and low-shear theories have emerged suggesting different biological pathways leading to formation and rupture, respectively.[4,5] Low WSS regions are often associated with aneurysmal rupture status,[3,6-10] possibly through

Key words
- Computational fluid dynamics
- Intracranial aneurysms
- Rupture status
- Velocity

Abbreviations and Acronyms
3D: Three-dimensional
AUC: Area under the curve
CFD: Computational fluid dynamics
ICA: Internal carotid artery
ROC: Receiver operating characteristic curve
WSS: Wall shear stress

Cerebrovascular Hemodynamics Laboratory, Department of Neurosurgery, Tufts Medical Center and Tufts University School of Medicine, Boston, Massachusetts, USA

To whom correspondence should be addressed: Adel M. Malek, M.D., Ph.D. [E-mail: amalek@tuftsmedicalcenter.org]

Citation: World Neurosurg. (2022) 158:e334-e343.
https://doi.org/10.1016/j.wneu.2021.10.178

Journal homepage: www.journals.elsevier.com/world-neurosurgery

Available online: www.sciencedirect.com

1878-8750/$ - see front matter © 2021 Elsevier Inc. All rights reserved.

flow stagnation inducing endothelial cell inflammation[11,12] in the dome.[3,13]

Given the ethical concerns involved in observing high-risk aneurysms, research on rupture risk has relied on retrospective databases, adopting rupture status discrimination as a surrogate for risk assessment, an approach that assumes aneurysm size and shape stability during rupture.[14,15] However, blebs appear prevalent in ruptured aneurysms,[16] often colocalize with the rupture site,[17-19] and are associated with both low WSS[18-21] and morphological changes following rupture.[7,17] Recent work introduced the possibility that blebs occur after rupture and are not always present beforehand.[22,23] Thus, there is a risk that retrospective rupture analysis based on local surface characteristics is less of a prediction tool and more of a self-fulfilling prophecy.

Volumetric analysis for rupture risk includes evaluation of flow pattern[24] and flow instability.[25] Velocity patterns are often used for visualization purposes, but velocity statistics have been less employed.[26,27] This study proposed a volumetric approach to rupture status prediction by evaluating the moments of the aneurysm velocity distribution with emphasis on robustness to surface irregularities and bleb presence to overcome the limitations of WSS-based techniques.

MATERIALS AND METHODS

Patient Selection

This research was approved by the institutional review board ethics committee. Patient consent was waived because of the retrospective nature of the study not impacting patient clinical care. High-resolution internal carotid artery (ICA) aneurysm three-dimensional (3D) catheter angiographic volumetric datasets, matched for size and age, were included if devoid of motion artifact. Inclusion criteria were met by 20 sidewall ICA aneurysms (10 ruptured) (**Figure 1**). All imaging of a ruptured subset was obtained within 48 hours from rupture to avoid vasospasm onset.

Data Processing

Angiographic volumes were analyzed and processed for segmentation using Amira visualization software platform version 5.3.3 (Thermo Fisher Scientific, Waltham, Massachusetts, USA) (**Figure 2A**). Vessel segmentation was performed with 3D gradient edge-detection filtering as previously described.[28] Three additional models were created to evaluate sensitivity to aneurysmal blebs and surface irregularities; ruptured aneurysms with focal small blebs were selected for bleb removal (**Figure 3**) using local Laplacian smoothing followed by surface reconstruction in MeshLab version 1.3.1 (ISTI-CNR, Pisa, Italy). Three additional unruptured aneurysms were selected for noise addition to the dome surface by fractal surface perturbation using the fractal Brownian motion algorithm (**Figure 4**).

Patient-Derived Models

All segmented surfaces (including bleb and noise analysis models) were used to create dynamic tetrahedral/prism meshes with boundary layer enhancement using ANSYS ICEM CFD (Ansys 19.2; ANSYS, Inc., Canonsburg, Pennsylvania, USA). The upstream parent vessel proximal to aneurysm was kept sufficiently long to enable full development of laminar flow and avoid entrance effects.

Computational Fluid Dynamics

Computational fluid dynamics (CFD) simulations were performed using Ansys 19.2, employing steady-state laminar flow with a Carreau non-Newtonian profile to approximate shear-dependent blood viscosity.[29] To account for variability in size, shape, and length of the parent vessel, inflow velocity was selected to obtain optimal parent vessel WSS conditions of 1.5 Pa upstream,[11] with zero gauge pressure at outlets.

Postprocessing analysis was performed using EnSight 10.2 (ANSYS, Inc.) (**Figure 1A** and **B**) by isolating the dome and exporting velocity values using the Brick of Values option, creating an isotropic discretization of the volume of interest. This led to a 256-cubed grid of equidistant float values, interpolated from meshing nodes, with a resulting mean voxel resolution of 0.033 ± 0.01 mm. This isometric sampling approach avoids the pitfalls of enriching velocity values in regions of higher mesh density (**Figure 1A** and **B**). Node-based WSS values were converted to element-based values for accurate spatial averaging, and the following features were extracted[6]: WSS aneurysm mean, WSS aneurysm minimum (average of 10 smallest WSS values to account for outliers), WSS aneurysm maximum (average of 10 largest WSS values to account for outliers), WSS 5% mean (spatial WSS mean of the 5% of total area covered by lowest WSS), and WSS 5% maximum (maximum WSS of the 5% of total area covered by lowest WSS).

Statistical Analysis

Velocity distribution statistics were extracted from the exported isometric sampling, and the following features were computed using MATLAB R2021 (The MathWorks, Inc., Natick, Massachusetts, USA): mean (first moment), variance (second moment), skewness (third moment), kurtosis (fourth moment), and standard deviation. Skewness describes the extent of asymmetry in the shape of a distribution. Positive skewness indicates a distribution concentrated on smaller values. A normal distribution has a skewness of 0, whereas an exponential distribution has a skewness value of 2. Kurtosis describes the tails of a distribution. A normal distribution has a kurtosis of 3, whereas an exponential distribution has a kurtosis of 9. Kurtosis values >3 (leptokurtic distributions) describe distributions with longer tails and more outliers compared with normal distributions.

JMP Pro 14 software (SAS Institute Inc., Cary, North Carolina, USA) was used to evaluate the performance of all velocity and WSS features in discriminating between ruptured and unruptured aneurysms using Student t test analysis with statistical significance assumed for $P < 0.05$. Receiver operating characteristic curve (ROC) analysis was performed, and prediction accuracy was evaluated using the area under the curve (AUC) index. Optimal threshold values were determined using ROC statistics. Multivariate logistic regression was performed separately, using forward stepwise regression on morphological features that achieved univariate statistical significance with a P value threshold of $P < 0.05$.

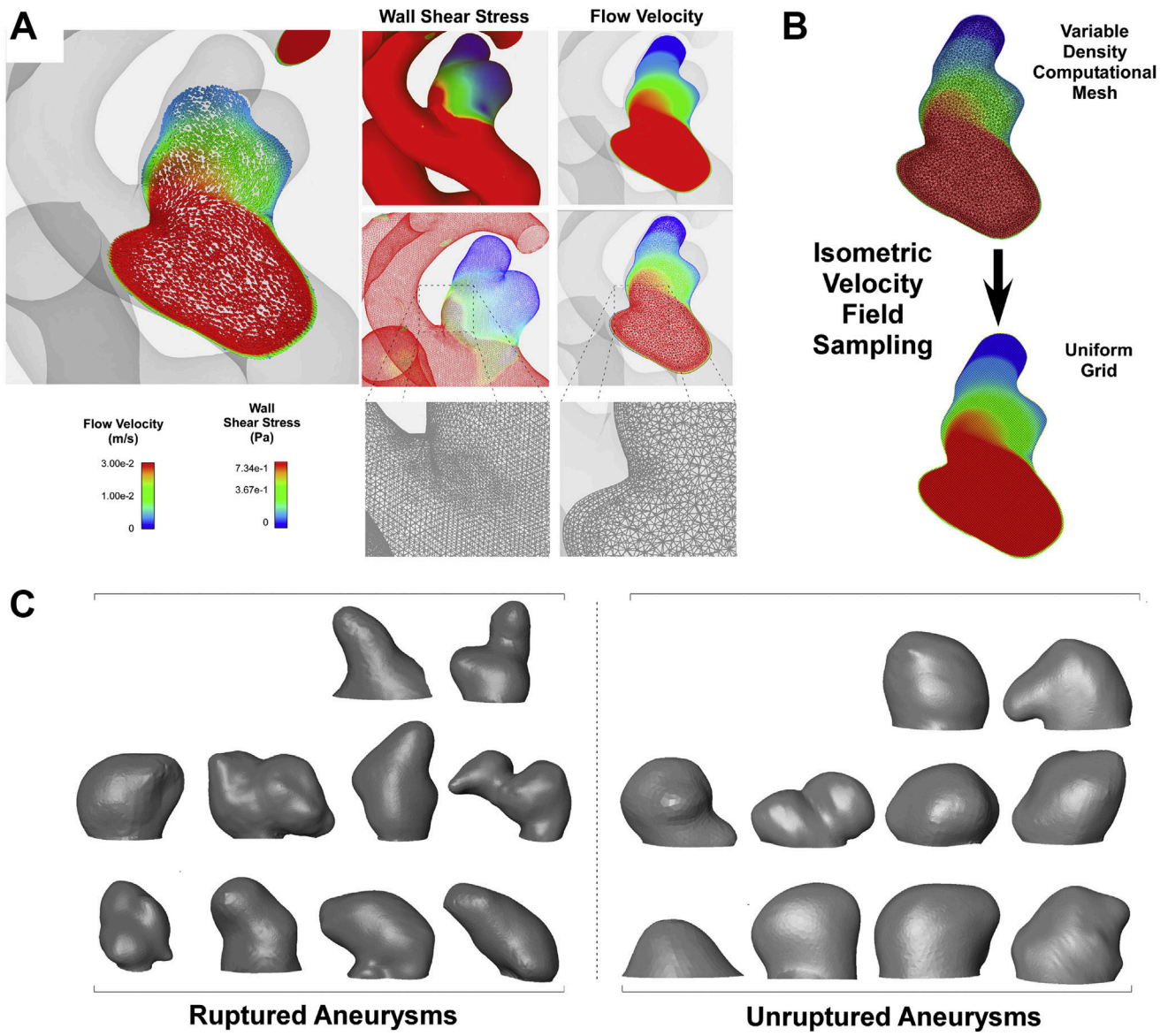


Figure 1. (**A**) Computational fluid dynamics models were created from segmented volumes, using adaptive meshing, with higher mesh density in areas of high curvature. Wall shear stress and velocity were evaluated in mesh-independent fashion. (**B**) Intra-dome velocity was exported as a grid of equidistant values, interpolated from meshing nodes. (**C**) Set of 10 ruptured and 10 unruptured aneurysms.

RESULTS

Video 1 provides a summary of our methodology and results.

Video

Video available at www.sciencedirect.com

Patient Demographics

3D rotational angiographic datasets from 20 patients (17 women) harboring sidewall ICA aneurysms were analyzed for the study. Before the study, 10 of the aneurysms were identified as ruptured aneurysms. There was no statistically significant age difference between patients with ruptured versus unruptured aneurysms (60.90 ± 12.22 years vs. 59.10 ± 13.12 years, $P = 0.75$) (Table 1), and domes were size matched with no significant difference in maximal dimension (10.21 ± 4.23 mm vs. 7.72 ± 3.30 mm, $P = 0.16$).

Dome Velocity Distribution and Wall Shear Analysis

Ruptured aneurysms had significantly lower mean velocity (0.019 ± 0.01 m/second vs. 0.038 ± 0.02 m/second, $P = 0.03$,

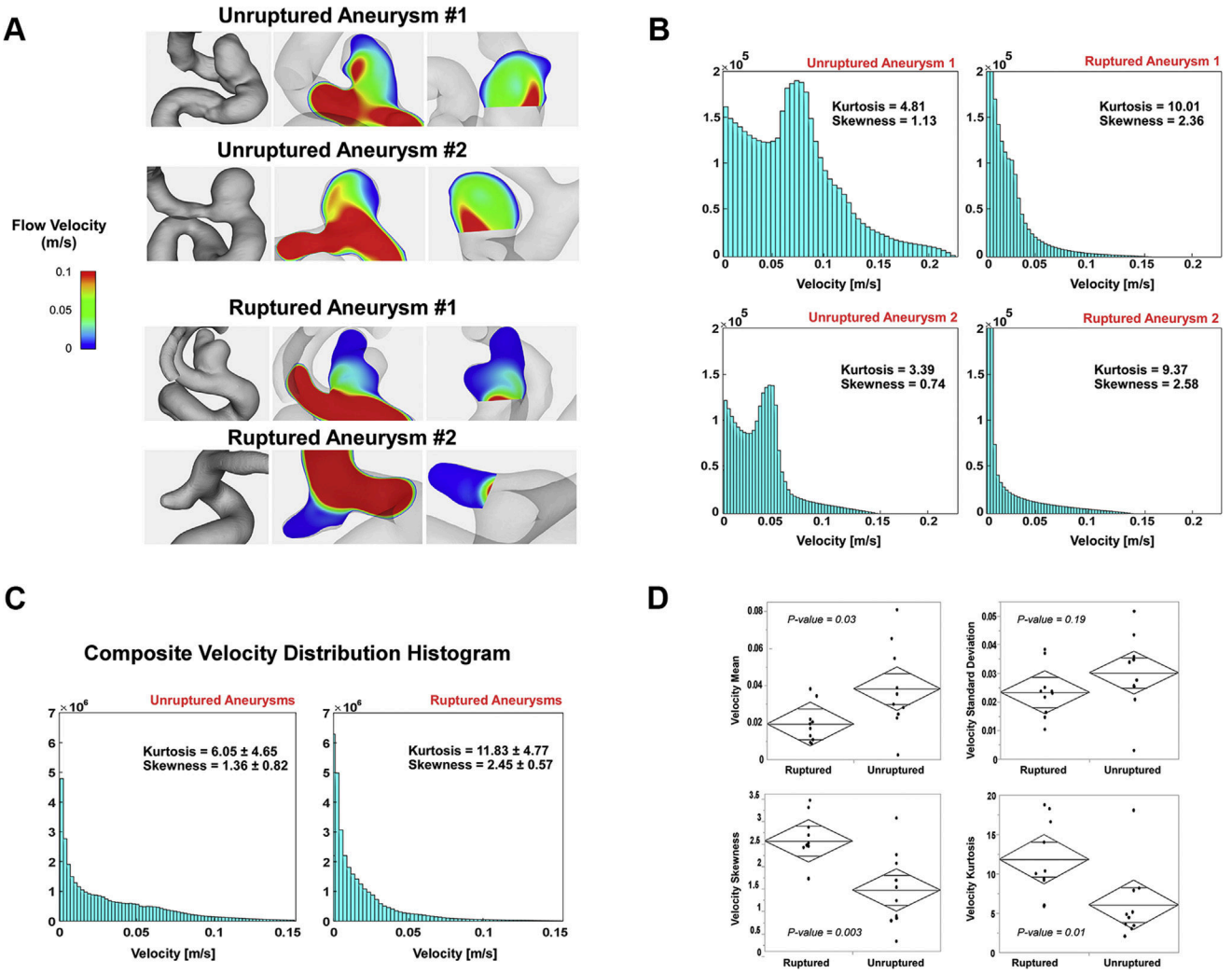
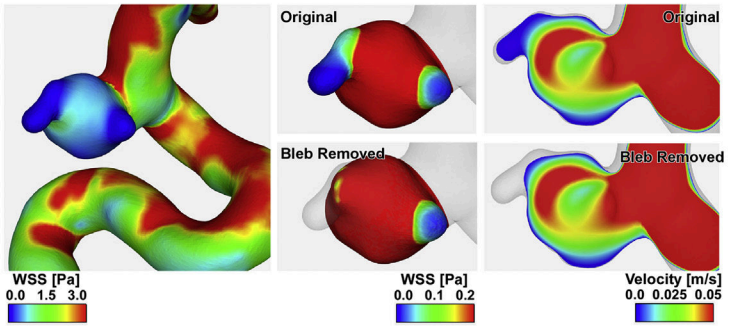


Figure 2. (**A**) Intra-dome velocity analysis of 2 unruptured and 2 ruptured sidewall internal carotid artery aneurysms. Details of velocity longitudinal and lateral cross sections through the aneurysm volume. (**B**) Velocity histograms corresponding to the 4 aneurysms. (**C**) Composite velocity histograms for all unruptured (left histogram) and ruptured (right histogram) aneurysms in the study. Velocity values were combined based on rupture status. Ruptured aneurysm velocity follows an exponential distribution. (**D**) Univariate analysis of the velocity distribution features (mean, standard deviation, skewness, and kurtosis).

AUC = 0.81) compared with the unruptured group (Table 1). Ruptured aneurysms showed significantly higher velocity skewness (2.45 ± 0.57 vs. 1.36 ± 0.82, P = 0.003, AUC = 0.88) and kurtosis (11.83 ± 4.77 vs. 6.05 ± 4.65, P = 0.01, AUC = 0.88) compared with unruptured aneurysms (Figure 2D). Based on ROC analysis, optimal predictive thresholds were identified for velocity kurtosis (threshold value 9.18, specificity 90%, and sensitivity 80%) and skewness (threshold value 2.31, specificity 90%, and sensitivity 80%). Maximum aneurysm velocity showed a trend toward being higher in the ruptured aneurysms, but variance and standard deviation were not significantly different between the groups. Eight ruptured aneurysms (80%) had skewness >2 and kurtosis >9, indicative of exponential distributions (Figure 2C). In contrast, only 2 unruptured aneurysms (20%) had skewness >2 and kurtosis >9. Forward selection multivariate analysis identified skewness alone as the best velocity-based rupture status predictor (AUC = 0.88).

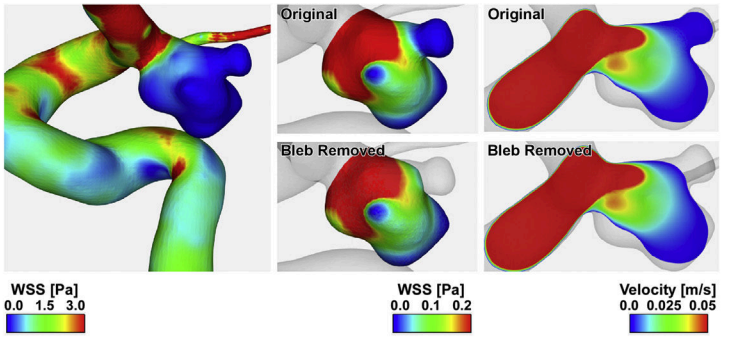
WSS univariate analysis showed that ruptured aneurysms had significantly lower minimum WSS (0.0015 ± 0.0024 Pa vs. 0.041 ± 0.031 Pa, P = 0.0008, AUC = 0.91) as well as lower WSS 5% mean (0.006 ± 0.007 Pa vs. 0.078 ± 0.058 Pa, P = 0.001, AUC = 0.90) and WSS 5% maximum (0.015 ± 0.022 Pa vs. 0.11 ± 0.09 Pa, P = 0.0005, AUC = 0.87). Based on ROC analysis, optimal predictive thresholds were identified for minimum WSS (threshold value 0.005, specificity 90%, and sensitivity 90%), WSS 5% mean

A



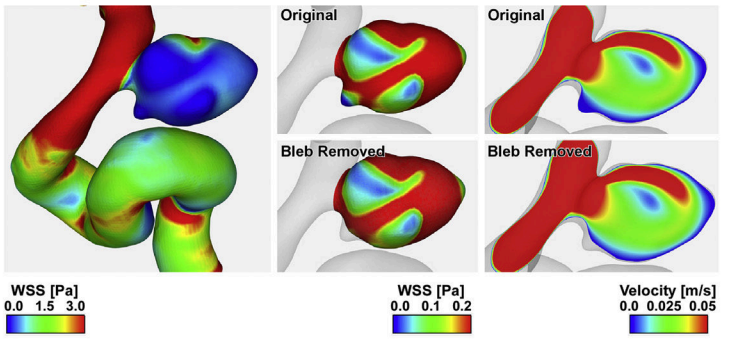
Model	WSS Minimum	WSS 5% Mean	Velocity Kurtosis	Velocity Skewness
Original with Bleb	0.0014 Pa	0.0036 Pa	8.598	1.901
Bleb Removed	0.0119 Pa	0.0400 Pa	8.205	1.839
% Change	750%	1011%	4.5%	3.3%

B



Model	WSS Minimum	WSS 5% Mean	Velocity Kurtosis	Velocity Skewness
Original with Bleb	0.0007 Pa	0.0013 Pa	11.259	2.475
Bleb Removed	0.0030 Pa	0.0106 Pa	10.838	2.409
% Change	329%	715%	3.7%	2.7%

C



Model	WSS Minimum	WSS 5% Mean	Velocity Kurtosis	Velocity Skewness
Original with Bleb	0.007 Pa	0.011 Pa	18.751	3.358
Bleb Removed	0.024 Pa	0.061 Pa	18.615	3.347
% Change	389%	487%	0.75%	0.32%

(threshold value 0.017, specificity 80%, and sensitivity 100%), and WSS 5% maximum (threshold value 0.024, specificity 80%, and sensitivity 90%).

Robustness to Bleb Presence

To evaluate the effect of the self-fulfilling prophecy of bleb presence in low WSS–based rupture discrimination techniques, bleb robustness analysis was performed on 3 ruptured aneurysms originally presenting with aneurysmal blebs. The blebs were digitally removed, and CFD analysis was repeated after bleb removal (Figure 3). Bleb removal resulted in a significant increase in the lower WSS, both for minimum WSS (0.0024 ± 0.0018 vs. 0.015 ± 0.0009, $P = 0.04$) and for WSS 5% mean (0.004 ± 0.005 vs. 0.03 ± 0.02, $P = 0.04$). There was no statistically significant change in any velocity statistics. The change was equivalent to 548% mean increase for minimum WSS and 887% increase for WSS 5% mean. In contrast, the velocity change between models with and without blebs was only 4.6% for skewness and 7% for kurtosis.

Not only did WSS values increase dramatically after bleb removal, but based on optimal threshold values, 2 of these 3 aneurysms became classified as unruptured using the WSS-based tool, with either low WSS or low 5% WSS (Figure 3A and C). In contrast, bleb removal had no effect on rupture status classification using the velocity tool on any of these 3 aneurysms.

Robustness to Surface Noise

Surface noise robustness analysis was performed on 3 unruptured aneurysms by adding surface irregularities using fractal surface perturbation (Figure 4). CFD analysis was repeated after noise addition. Surface irregularities induced significant decrease of the minimum WSS values (0.048 ± 0.012 vs. 0.007 ± 0.006, $P = 0.007$) and a decreasing trend for WSS 5% mean (0.08 ± 0.011 vs. 0.039 ± 0.024, $P = 0.06$). There was no statistically significant change in any velocity statistics (Figure 3D). Noise addition resulted in 85.9% mean decrease for minimum WSS and 50.9% decrease for WSS 5% mean. In contrast, the velocity change between models with and without noise was only 4.8% for skewness and 3.4% for kurtosis.

Not only did WSS values decrease with noise addition, but based on optimal threshold values of low WSS, 1 of the 3 aneurysms changed rupture status classification from unruptured to ruptured (Figure 4C). In contrast, noise addition had no such effect on rupture status classification using the velocity distribution moment tool in any of the 3 aneurysms.

DISCUSSION

CFD simulations are increasingly used to provide insight into the mechanisms of aneurysm rupture.[1,10] Surface-based approaches focus on dome WSS statistics,[3-9] with many studies reporting significantly lower WSS in ruptured aneurysms, particularly in areas of low flow.[3,6-10] Volumetrically, analysis based on velocity visualization of flow patterns are often used,[24,30] but quantitative analysis based on dome velocity statistics are less commonly employed for rupture status classification. Detmer et al.[26] evaluated mean, peak velocity, and time averaged maximum velocity in the dome, finding higher peak velocities in ruptured cases; similar higher maximum velocity was reported in ruptured lesions by Chung at al.[27] Intra-aneurysmal velocity distribution has been evaluated on four-dimensional phase-contrast magnetic resonance angiography,[31] showing some differences in aneurysm types but not in classifying rupture status. The current study relied on much higher spatial resolution of catheter 3D rotational angiographic datasets combined with CFD.

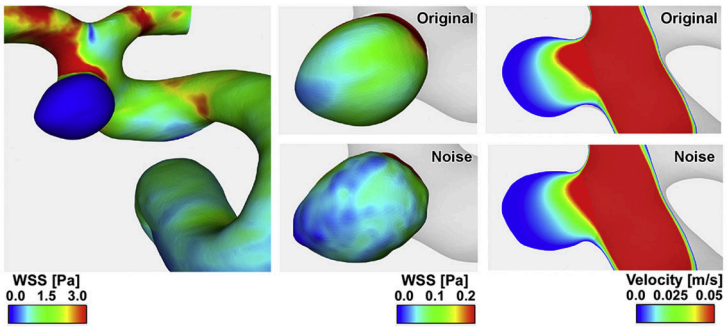
This study focused on 3D rotational angiographic data and proposed a volumetric approach to rupture status classification by evaluating the moments of aneurysm dome velocity distribution, relying on a mesh-independent isometric sampling of the velocity, resulting in mesh density–independent results. This is a critical feature for computing the moments of the velocity distribution as opposed to evaluating spatial means because computational meshes and volumes representing the surface and flow volume are routinely computed with high variable mesh densities around areas of curvature and near boundaries to enhance computational efficiency and accuracy. Simply sampling the entirety of these elements would distort the velocity distribution based on local computational mesh density.

Analysis of velocity moments showed ruptured aneurysms to have lower mean values, but higher skewness (2.45 vs. 1.36) and kurtosis (11.83 vs. 6.05) compared with unruptured aneurysms. The moments describe the shape of a distribution, with skewness describing the asymmetry and kurtosis describing the tails of the distribution. Our results show that ruptured aneurysms have exponential velocity distributions (skewness >2 and kurtosis >9) skewed toward low velocity values, indicative of aneurysm low flow. In univariate and multivariate statistical analysis, skewness emerged as best velocity-based predictor of rupture with an AUC of 0.88.

Velocity-based analysis was compared with WSS evaluation on the aneurysmal surface. Similar to prior work,[3,6-10] ruptured aneurysms had significantly lower WSS, particularly in areas covered by low WSS values. Minimum WSS (computed as the average of the 10 smallest WSS values to avoid minimum outliers) emerged as best WSS predictor with an AUC of 0.91. Despite its classifier performance, WSS was previously shown to be sensitive to acquisition modality and reconstruction characteristics.[32] In addition, low WSS was previously associated with bleb presence.[19-21] Not only were blebs shown to be prevalent in

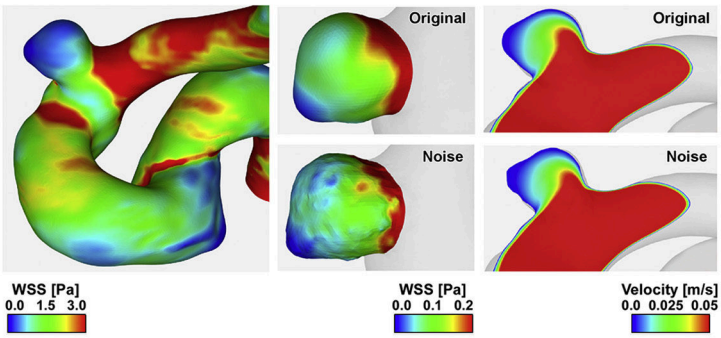
Figure 3. (**A**–**C**) Computational fluid dynamics simulations on 3 ruptured aneurysms with original blebs and after bleb removal. Details on wall shear stress on aneurysm surface and on velocity on longitudinal cross section through the aneurysm volume. Bleb removal resulted in significant increase in both minimum wall shear stress and lowest 5% wall shear stress, but no significant change in velocity features. WSS, wall shear stress.

A



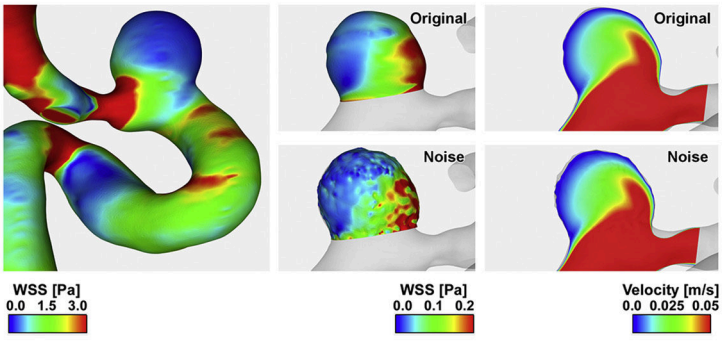
Model	WSS Minimum	WSS 5% Mean	Velocity Kurtosis	Velocity Skewness
Original	0.0590 Pa	0.0827 Pa	6.313	1.851
Noise	0.032 Pa	0.0171Pa	6.680	1.928
% Change	94.5%	79.3%	5.8%	4.2%

B



Model	WSS Minimum	WSS 5% Mean	Velocity Kurtosis	Velocity Skewness
Original	0.053 Pa	0.068 Pa	3.018	0.831
Noise	0.014 Pa	0.037Pa	3.083	0.888
% Change	74.1%	45.9%	2.1%	6.8%

C



Model	WSS Minimum	WSS 5% Mean	Velocity Kurtosis	Velocity Skewness
Original	0.0347 Pa	0.091 Pa	5.147	1.438
Noise	0.0037 Pa	0.065 Pa	5.270	1.492
% Change	89.1%	27.8%	2.4%	3.7%

Table 1. Univariate Statistical Analysis of Wall Shear Stress and Velocity Distribution Parameters

	Ruptured (n = 10)	Unruptured (n = 10)	P Value	AUC
Age, years	60.90 ± 12.22	59.10 ± 13.12	0.75	0.53
Maximal size, mm	10.21 ± 4.23	7.72 ± 3.30	0.16	0.71
Velocity mean, m/second	0.019 ± 0.01	0.038 ± 0.02	0.03*	0.81
Velocity max, m/second	0.17 ± 0.07	0.16 ± 0.05	0.58	0.51
Velocity SD, m/second	0.023 ± 0.009	0.03 ± 0.013	0.19	0.71
Velocity kurtosis	11.83 ± 4.77	6.05 ± 4.65	0.01*	0.88
Velocity skewness	2.45 ± 0.57	1.36 ± 0.82	0.003*	0.88
WSS aneurysm mean, Pa	0.31 ± 0.17	0.50 ± 0.29	0.08	0.74
WSS aneurysm max, Pa	8.73 ± 8.81	6.37 ± 5.26	0.47	0.50
WSS aneurysm min, Pa	0.0015 ± 0.0024	0.041 ± 0.031	0.0008*	0.91
WSS 5% mean, Pa	0.006 ± 0.007	0.078 ± 0.058	0.001*	0.90
WSS 5% max, Pa	0.015 ± 0.022	0.11 ± 0.09	0.005*	0.87

Values are presented as mean ± SD.
AUC, area under the curve; max, maximum; SD, standard deviation; WSS, wall shear stress; min, minimum.
*Statistical significance (assumed for $P < 0.05$).

ruptured aneurysms[16] and to colocalize with the rupture site,[17-19] but recent research raised the question of whether some of the blebs are in fact rupture-induced morphological changes and not part of the prerupture morphology.[22,23] In imaging assessments before and after rupture, Yi et al.[23] showed new daughter sacs emerging after rupture in 5 of 6 patients studied. Similarly, Skodvin et al.[22] showed increased fraction of aneurysms with blebs from 31% before rupture to 59% after rupture. It is possible that bleb emergency by rupture might result in increased areas of low WSS contributing to the predictive power of WSS in rupture status classification. Indeed, bleb removal resulted in a 10-fold increase in minimum WSS, altering WSS-based classification of 2 of 3 aneurysms from ruptured to unruptured following bleb removal. In contrast, bleb removal had minimal impact on dome velocity skewness and kurtosis and no effect on velocity-based rupture classification.

Robustness to surface noise analysis was performed through surface perturbations to 3 unruptured aneurysms. Being a spatial derivative of the velocity, WSS will always be inherently more sensitive to noise than velocity.[33] Noise addition decreased dome WSS values, with minimal impact on velocity skewness and kurtosis. Based on optimal WSS threshold values, 1 of the 3 aneurysms changed rupture status from unruptured to ruptured after noise addition, with no change in classification when using dome velocity skewness and kurtosis.

Study Limitations

This study was retrospective and used for classification of previous rupture status, rather than prediction. Retrospective analysis depends on the hypothesis that aneurysms do not change size and shape after rupture. Conclusive data on this subject remain to be found, but this study shows that even with postrupture morphology changes, such as bleb occurrence, some predictive features might be robust to these changes. These results were evaluated on 20 volume-matched ICA sidewall aneurysms to avoid confounding factors, such as morphological differences between sidewall and bifurcation lesions[34] and hemodynamic differences between small and large aneurysms.[35] In addition, this study evaluated a relatively small dataset of 10 ruptured and 10 unruptured aneurysms. Validation of the results on a larger dataset with aneurysms of different sizes and from multiple locations and considering clinical history and examination (e.g., arterial hypertension, smoking, alcohol consumption, family history of aneurysmal subarachnoid hemorrhage) will be the focus of future investigation. CFD simulations were performed under steady-state inflow conditions, which represent an approximation of the flow characteristics throughout the cardiac cycle. Although researchers have argued that less computationally intensive steady flow simulations provide relevant hemodynamic information,[36] for clinical relevance to be established, these findings will require validation on larger datasets under pulsatile flow simulations.

Figure 4. (**A**–**C**) Computational fluid dynamics simulations on 3 unruptured aneurysms after noise addition. Details on wall shear stress on aneurysm surface and on velocity on longitudinal cross section through the aneurysm volume. Noise addition to the surface resulted in significant decrease in minimum wall shear stress, but no significant change in velocity moment features. WSS, wall shear stress.

CONCLUSIONS

This study proposed a volumetric approach to rupture status classification by evaluating the moments of dome velocity distribution in 20 (10 ruptured) volume-matched sidewall aneurysms, employing mesh-independent isometric sampling. Moments of the velocity distribution within the aneurysm dome are strong predictors of rupture status. Skewness emerged as the best statistical performer with an AUC of 0.88. Ruptured aneurysms show exponential velocity distributions with high peaks (high kurtosis) at low values (high skewness) indicative of aneurysm low flow and stagnation. Velocity-based analysis was compared with WSS evaluation on the surface dome, and robustness to surface irregularities and noise was performed for surface and volume-based parameters. In contrast to low WSS, which was shown to be sensitive to bleb presence or surface irregularities and noise, isometrically sampled velocity statistics were found to be robust to both. These findings will require validation in prospective studies before clinical application in risk assessment of incidental aneurysms.

CRediT AUTHORSHIP CONTRIBUTION STATEMENT

Alexandra Lauric: Acquisition of data, Image processing, Formal analysis, Data curation, Writing — original draft. **James E. Hippelheuser:** Acquisition of data, Image processing. **Adel M. Malek:** Conceptualization, Methodology, Acquisition of data, Formal analysis, Data curation, Writing — review & editing, Final approval.

REFERENCES

1. Sforza DM, Putman CM, Cebral JR. Hemodynamics of cerebral aneurysms. *Annu Rev Fluid Mech*. 2009;41:91-107.
2. Sheikh MAA, Shuib AS, Mohyi MHH. A review of hemodynamic parameters in cerebral aneurysm. *Interdiscip Neurosurg*. 2020;22:100716.
3. Kadasi LM, Dent WC, Malek AM. Colocalization of thin-walled dome regions with low hemodynamic wall shear stress in unruptured cerebral aneurysms. *J Neurosurg*. 2013;119:172-179.
4. Meng H, Tutino VM, Xiang J, Siddiqui A. High WSS or low WSS? Complex interactions of hemodynamics with intracranial aneurysm initiation, growth, and rupture: toward a unifying hypothesis. *AJNR Am J Neuroradiol*. 2014;35:1254-1262.
5. Machi P, Ouared R, Brina O, et al. Hemodynamics of focal versus global growth of small cerebral aneurysms. *Clin Neuroradiol*. 2019;29:285-293.
6. Lauric A, Hippelheuser J, Cohen AD, Kadasi LM, Malek AM. Wall shear stress association with rupture status in volume matched sidewall aneurysms. *J Neurointerv Surg*. 2014;6:466.
7. Kono K, Fujimoto T, Shintani A, Terada T. Hemodynamic characteristics at the rupture site of cerebral aneurysms: a case study. *Neurosurgery*. 2012;71:E1202-E1209.
8. Miura Y, Ishida F, Umeda Y, et al. Low wall shear stress is independently associated with the rupture status of middle cerebral artery aneurysms. *Stroke*. 2013;44:519-521.
9. Suzuki T, Stapleton CJ, Koch MJ, et al. Decreased wall shear stress at high-pressure areas predicts the rupture point in ruptured intracranial aneurysms. *J Neurosurg*. 2019;132:1116-1122.
10. Zhou G, Zhu Y, Yin Y, Su M, Li M. Association of wall shear stress with intracranial aneurysm rupture: systematic review and meta-analysis. *Sci Rep*. 2017;7:5331.
11. Malek AM, Alper SL, Izumo S. Hemodynamic shear stress and its role in atherosclerosis. *JAMA*. 1999;282:2035-2042.
12. Aoki T, Yamamoto K, Fukuda M, Shimogonya Y, Fukuda S, Narumiya S. Sustained expression of MCP-1 by low wall shear stress loading concomitant with turbulent flow on endothelial cells of intracranial aneurysm. *Acta Neuropathol Commun*. 2016;4:48.
13. Kadasi LM, Dent WC, Malek AM. Cerebral aneurysm wall thickness analysis using intraoperative microscopy: effect of size and gender on thin translucent regions. *J Neurointerv Surg*. 2013;5:201-206.
14. Rahman M, Ogilvy CS, Zipfel GJ, et al. Unruptured cerebral aneurysms do not shrink when they rupture: multicenter collaborative aneurysm study group. *Neurosurgery*. 2011;68:155-160 [discussion: 160-161].
15. Asari S, Ohmoto T. Natural history and risk factors of unruptured cerebral aneurysms. *Clin Neurol Neurosurg*. 1993;95:205-214.
16. Tsukahara T, Murakami N, Sakurai Y, et al. Treatment of unruptured cerebral aneurysms; a multi-center study at Japanese national hospitals. *Acta Neurochir Suppl*. 2005;94:77-85.
17. Lauric A, Heller RS, Schimansky S, Malek AM. Benefit of cone-beam CT angiography in visualizing aneurysm shape and identification of exact rupture site. *J Neuroimaging*. 2015;25:56-61.
18. Salimi Ashkezari SF, Mut F, Chung BJ, et al. Hemodynamics in aneurysm blebs with different wall characteristics. *J Neurointerv Surg*. 2021;13:642-646.
19. Li M, Wang J, Liu J, Zhao C, Yang X. Hemodynamics in ruptured intracranial aneurysms with known rupture points. *World Neurosurg*. 2018;118:e721-e726.
20. Kawaguchi T, Nishimura S, Kanamori M, et al. Distinctive flow pattern of wall shear stress and oscillatory shear index: similarity and dissimilarity in ruptured and unruptured cerebral aneurysm blebs. *J Neurosurg*. 2012;117:774-780.
21. Cebral JR, Sheridan M, Putman CM. Hemodynamics and bleb formation in intracranial aneurysms. *AJNR Am J Neuroradiol*. 2010;31:304-310.
22. Skodvin TØ, Johnsen LH, Gjertsen Ø, Isaksen JG, Sorteberg A. Cerebral aneurysm morphology before and after rupture. *Stroke*. 2017;48:880-886.
23. Yi J, Zielinski D, Chen M. Cerebral aneurysm size before and after rupture: case series and literature review. *J Stroke Cerebrovasc Dis*. 2016;25:1244-1248.
24. Cebral JR, Castro MA, Burgess JE, Pergolizzi RS, Sheridan MJ, Putman CM. Characterization of cerebral aneurysms for assessing risk of rupture by using patient-specific computational hemodynamics models. *AJNR Am J Neuroradiol*. 2005;26:2550-2559.
25. Valen-Sendstad K, Mardal KA, Steinman DA. High-resolution CFD detects high-frequency velocity fluctuations in bifurcation, but not sidewall, aneurysms. *J Biomech*. 2013;46:402-407.
26. Detmer FJ, Chung BJ, Mut F, et al. Development of a statistical model for discrimination of rupture status in posterior communicating artery aneurysms. *Acta Neurochir*. 2018;160:1643-1652.
27. Chung BJ, Mut F, Putman CM, et al. Identification of hostile hemodynamics and geometries of cerebral aneurysms: a case-control study. *AJNR Am J Neuroradiol*. 2018;39:1860-1866.
28. Baharoglu MI, Lauric A, Wu C, Hippelheuser J, Malek AM. Deviation from optimal vascular caliber control at middle cerebral artery bifurcations harboring aneurysms. *J Biomech*. 2014;47:3318-3324.
29. Schirmer CM, Malek AM. Wall shear stress gradient analysis within an idealized stenosis using non-Newtonian flow. *Neurosurgery*. 2007;61:853-863 [discussion: 863-864].
30. Futami K, Kitabayashi T, Sano H, et al. Inflow jet patterns of unruptured cerebral aneurysms based on the flow velocity in the parent artery: evaluation using 4D flow MRI. *AJNR Am J Neuroradiol*. 2016;37:1318-1323.
31. Schnell S, Ansari SA, Vakil P, et al. Three-dimensional hemodynamics in intracranial aneurysms: influence of size and morphology. *J Magn Reson Imaging*. 2014;39:120-131.
32. Lauric A, Hippelheuser JE, Malek AM. Critical role of angiographic acquisition modality and reconstruction on morphometric and haemodynamic analysis of intracranial aneurysms. *J Neurointerv Surg*. 2018;10:911-915.
33. Tsou JK, Jie L, Pellot-Barakat C, Insana MF. Improved accuracy of vascular wall shear rate

measurements. *Proceedings of the IEEE Ultrasonics Symposium*. 2004;2:1239-1242.

34. Baharoglu MI, Lauric A, Gao BL, Malek AM. Identification of a dichotomy in morphological predictors of rupture status between sidewall- and bifurcation-type intracranial aneurysms. *J Neurosurg*. 2012;116:871-881.

35. Varble N, Tutino VM, Yu J, et al. Shared and distinct rupture discriminants of small and large intracranial aneurysms. *Stroke*. 2018;49:856-864.

36. Cebral JR, Mut F, Weir J, Putman C. Quantitative characterization of the hemodynamic environment in ruptured and unruptured brain aneurysms. *AJNR Am J Neuroradiol*. 2011;32:145-151.

Conflict of interest statement: The authors declare that the article content was composed in the absence of any commercial or financial relationships that could be construed as a potential conflict of interest.

Received 12 July 2021; accepted 27 October 2021

Citation: World Neurosurg. (2022) 158:e334-e343.
https://doi.org/10.1016/j.wneu.2021.10.178

Journal homepage: ***www.journals.elsevier.com/world-neurosurgery***

Available online: ***www.sciencedirect.com***

1878-8750/$ - see front matter © 2021 Elsevier Inc. All rights reserved.